Infrared Laser Desorption of Hydroquinone from a Water−Ethanol Liquid Beam

Dale E. Otten, Adam J. Trevitt, Benjamin D. Nichols, Gregory F. Metha, and Mark A. Buntine*

Department of Chemistry, The University of Adelaide, Adelaide SA 5005, Australia

Received: October 17, 2002; In Final Form: May 6, 2003

We have investigated the 1.9-μm IR desorption of hydroquinone in a water/ethanol liquid beam under relatively high desorption laser fluences (1316 and 2632 mJ cm^{-2} pulse^{-1}). The appearance of the IR desorption/UV ionization TOF mass spectrum of hydroquinone (HQ) is interpreted in terms of dissociation of solvated HQ clusters during the ionization event. The maximum in the hydroquinone desorption velocity distribution is 300 ms^{-1}, and the translational temperature of the desorbed species is approximately 1500 K. We see no evidence for an acoustic compression−ejection mechanism, suggesting that such a process is operative at desorption laser fluences lower than employed here. Our results suggest a general mechanism for the high-powered IR desorption from a liquid beam whereby desorbed species are ejected into the vacuum possessing considerable translational energy but remain internally cool.

1. Introduction

An in vacuo liquid microjet (LμJ), or "liquid beam", is formed when a liquid sample is injected through a thin aperture or capillary at relatively high speed directly into a vacuum. Liquid-beam techniques have gained in popularity over the past decade, with recent advances providing valuable experimental insight into molecular dynamics at the liquid−vacuum interface.[1]

In the past few years, liquid-beam techniques have been developed to introduce nonvolatile compounds into the gas phase for mass spectrometric interrogation. One motivation for this development has been to overcome the problem of thermal decomposition of many low- or nonvolatile compounds when heated, in attempts to introduce these species into the gas phase. Studies by Brutschy[2−10] and Kondow[11−13] suggest that liquid-beam injection techniques, coupled with IR laser desorption, are well suited to isolating (solvated) nonvolatile molecules from bulk solution.

Brutschy and co-workers use a moderate-to-high powered pulsed IR laser to rapidly heat a liquid beam and drive preformed biomolecular ions into the vacuum.[14] These workers show mass spectrometric evidence that the IR laser desorption of several different proteins in solution preserves the noncovalent interactions within and between biomolecules and the solvent. Kondow's group has investigated the gas-phase microsolvation dynamics of hydrated small molecule clusters via IR irradiation of aqueous liquid beams. In Kondow's experiments, neutral nonvolatile solute molecules and their hydrated clusters are liberated from solution prior to subsequent ionization by a separate UV laser pulse that passes by the liquid beam.

Seminal work from Kondow's laboratory has shown that in using pulsed 1.9-μm radiation to desorb hydrated clusters of the low volatility molecule resorcinol, *meta*-$C_6H_4(OH)_2$, from aqueous solution, two different isolation mechanisms operate.[11,12] The 1.9-μm radiation is resonant with the (0,1,1) vibrational combination band in liquid water and therefore most likely only excites the solvent molecules within the liquid beam. Following the IR irradiation pulse, in the early time domain ($<\sim$500 ns) fast moving, internally cold clusters are ejected, while in the late time domain ($>\sim$5 μs) only slow moving, thermalized bare solute molecules are observed. Kondow interprets these results in terms of an initial compression (sound) wave rapidly ejecting material from the surface of the liquid beam, followed by a relatively long evaporative process brought about by delocalization of the IR energy heating the liquid sample.

In a subsequent study involving the desorption of phenol molecules from aqueous solution using 2.92-μm IR radiation (corresponding to a fundamental OH stretch vibrational band in liquid water), Kondow observes only one isolation mechanism involving hydrated cluster ejection over a several microsecond time period.[13] The rapid ejection process is not observed. Kondow attributes this absence to the relatively low 2.92-μm IR laser fluence employed compared to the earlier 1.9-μm IR desorption studies. However, on the basis of Kondow's reported experimental conditions where the 2.92-μm studies employed significantly tighter focusing conditions,[11−13] we calculate the 1.9-μm desorption laser fluence to be $\sim$130 mJ cm^{-2} pulse^{-1} whereas the 2.92-μm desorption laser fluence is reported to be $\sim$1100 mJ cm^{-2} pulse^{-1}. In other words, the rapid ejection process would appear to become inoperative at higher desorption laser fluences.

Most recently, Kondow has reported the generation of neutral water clusters, $(H_2O)_n$, $n > 56$, following IR irradiation at 2.96 μm.[15] In this study, a bimodal neutral water cluster velocity distribution is observed over a range of intense IR irradiation powers from 4.5 to 7 mJ/pulse. The bimodal distribution is interpreted in terms of clusters being ejected from the liquid-beam surface (fast clusters) or from the bulk of the water beam (slow clusters). Of most relevance here, however, is the observation that the abundance of the "fast" desorption component barely increases, whereas the abundance of the "slow"

* Address correspondence to this author. Fax: +61-8-8303-4358; e-mail: mark.buntine@adelaide.edu.au.

10.1021/jp022248b CCC: $25.00
Published on Web 07/19/2003

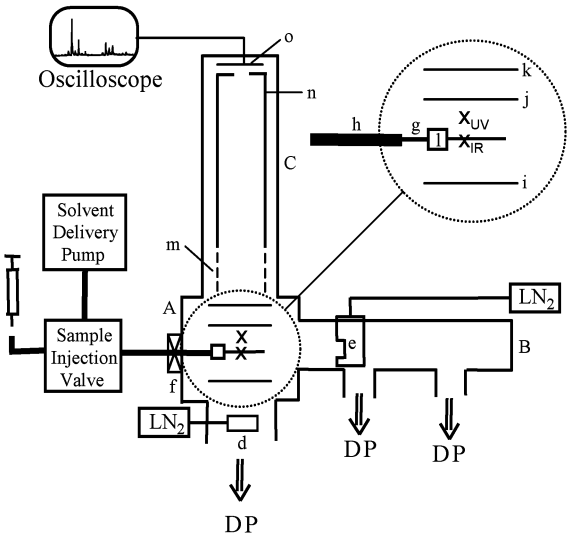

Figure 1. A schematic illustration of the liquid microjet (LμJ) apparatus coupled to a TOF mass spectrometer. The apparatus consists of a source chamber (A), a condensation chamber (B), and a TOF chamber (C). See text for an explanation of the key features of the instrument and for the details of operation.

component increases rapidly with IR irradiation power. Clearly, the IR laser fluence plays an important role in the desorption process.

In the present study, as a complement to the studies by Kondow, we report the results of an investigation into the 1.9-μm IR desorption of the nonvolatile molecule hydroquinone, *para*-$C_6H_4(OH)_2$, from a water−ethanol liquid beam under relatively high-powered pulsed desorption laser conditions. Under the experimental conditions employed in this study, we see no evidence for the acoustic compression−ejection process. Indeed, we show that the maximum in the desorption velocity distribution is more than 5 times slower than the speed of sound in an ethanol−water solution. Our results support the putative notion that the acoustic compression−ejection model may only be operative under relatively low-powered IR desorption conditions.

We also compare, under otherwise near identical experimental conditions, the time-of-flight mass spectrum of hydroquinone ionized via UV multiphoton absorption following desorption from a liquid beam (a thermodynamic nonequilibrium process) with that of molecules ionized following evaporation from the liquid surface (a thermodynamic equilibrium process) and discuss the role of solvated cluster dissociation on the appearance of the desorption mass spectrum.

2. Experimental Section

The experimental apparatus is similar, although not identical, to that previously described.[16] A schematic illustration of the LμJ apparatus coupled to a TOF mass spectrometer is presented in Figure 1. The apparatus consists of a source chamber (A), a condensation chamber (B), and a TOF chamber (C). The source chamber is equipped with a cryotrapped Varian VHS-6 2400 L/s diffusion pump. The condensation chamber is pumped by two Edwards Model E02, 150 L/s diffusion pumps and the TOF chamber is pumped by a second cryotrapped Varian VHS-6 diffusion pump. When the LμJ is in operation, the pressure in the source chamber is typically $10^{-4}-10^{-5}$ Torr, depending on the liquid flow rate. Lower source chamber pressures are maintained by cooling a 5-cm diameter copper cup placed above the throat of the diffusion pump with liquid nitrogen (d). Approximately 8-cm downstream from the nozzle, the LμJ passes into the condensation chamber. Here, a 15-cm diameter cylindrical stainless steel trap modified to include a solid-waste collection cavity (e) and filled with liquid nitrogen acts as a liquid waste cryropumping/condensation unit. Typically, the LμJ can be operated for approximately 3 h before the condensation traps need to be removed and cleaned.

The LμJ assembly enters the source chamber via a gate valve interlock (f). The LμJ assembly consists of a 3-cm length of 25-μm internal diameter fused silica capillary tubing (g) attached to 0.51-mm internal diameter stainless steel chromatography tubing (h). A constant flow of liquid through the LμJ capillary is supplied and maintained by a conventional liquid chromatography solvent delivery pump (Waters Model 590). The pump is fitted with flow-dampening modules to minimize oscillations in the flow rate. A 0.2-micron porous filter designed to prevent clogging of the nozzle aperture is placed in series with the flow-dampening modules. Liquid flow rates of between 0.2 and 1.0 mL/min are used throughout. One milliliter sample solutions are injected into the continuous liquid flow using a Reodyne chromatography injection valve (Model 7725i) fitted with a 1-mL sample loop. The 3-cm channel length of the LμJ capillary (g) allows for laminar flow conditions to be established prior to the liquid jet entering the vacuum chamber.[17] The fused silica tubing used in these experiments is readily available as a relatively inexpensive gas chromatography consumable.

Approximately 12-mm downstream from the nozzle aperture, the LμJ is intersected at right angles (into the plane of the page in Figure 1) by a gently focused 1.9-μm IR laser pulse. The annotation (X_{IR}) denotes the IR laser interaction region downstream from the nozzle aperture in Figure 1. The IR laser focal spot size is 220 μm, with irradiation powers of either 1316 mJ cm^{-2} $pulse^{-1}$ (0.19 GW/cm^2) or 2632 mJ cm^{-2} $pulse^{-1}$ (0.38 GW/cm^2).

The 1.9-μm radiation is generated as the first Stokes Raman-shifted wavelength from the fundamental (1064 nm) output of a pulsed Nd:YAG laser (Quanta Ray GCR-170−10) passed through a 1-m-long home-built Raman cell filled with H_2 at a pressure of 2070 kPa. The 1064-nm YAG beam was gently focused midway along the Raman cell with a 700-mm focal length plano−convex lens. Output from the Raman cell was re-collimated with a 600-mm focal length plano−convex lens.

The IR irradiation liberates neutral molecules from the liquid microjet into the vacuum of the source chamber. Solute (hydroquinone) molecules ejected along the TOF axis are ionized by a gently focused 266-nm laser beam whose propagation axis is parallel to the IR laser beam but translated 0.3 mm away from the liquid microjet toward the TOF detector. The UV laser interaction region is denoted by the annotation (X_{UV}) in Figure 1.

The 266-nm laser radiation is generated by externally doubling the 532-nm output from a pulsed Nd:YAG laser (Big Sky Laser, ULTRA-CFR). In our earlier report,[16] the UV laser output (typically 220−260 μJ/pulse) was focused by a plano−convex lens with a focal length of 250 mm, resulting in laser fluences of ~2.5 GW/cm^2 at the focal region.[18] In the present study, slightly gentler photoionization conditions of 0.69 GW/cm^2 (855 μJ/pulse into a 150-μm focal spot size) were employed. We have previously shown that in the power regime of 2−7 GW/cm^2, the relative intensity distribution of the hydroquinone parent and fragment ions remains constant.[16]

The ultraviolet laser radiation ionizes the solute hydroquinone molecules via 1+1 resonance-enhanced multiphoton ionization (REMPI) and the nascent solute ions are accelerated out of the

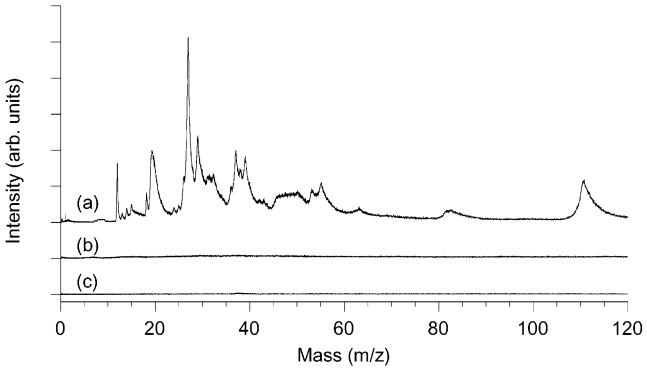

Figure 2. (a) IR (1.9-μm) desorption/UV (266-nm) ionization TOF mass spectrum of a 10^{-2} M solution of hydroquinone in 25% v/v ethanol in water. (b) TOF mass spectrum recorded under identical conditions to the top trace, except that the UV laser is blocked. The lack of signal confirms that IR multiphoton ionization is not contributing to the ion signal in the top trace. (c) TOF mass spectrum recorded under identical conditions to the top trace, except that the IR laser is blocked. The lack of signal confirms that UV multiphoton ionization of solute evaporating from the surface of the liquid beam is not contributing to the ion signal in the top trace. See text for a complete discussion.

source chamber by a two-stage static electric field generated between three ion extraction plates. The first two plates (i and j) are separated by 3 cm. The LμJ aperture is situated midway between these two plates. For the positive ion detection mode discussed here, the rear plate (i) is maintained at +2.5 kV while the middle plate (j) is maintained at +1.2 kV. The third ion plate (k), maintained at ground potential, is separated from the middle plate by a further 2 cm. To maintain a uniform electric field between the first-stage ion extraction plates, the LμJ capillary passes through a small brass block (l) charged at +2.0 kV. The charged brass block prevents distortions of the ion-extraction field attributable to the electrically grounded fused silica capillary being located between the two charged plates.

Entering the TOF chamber, the fast-moving ions pass through a series of ion focusing and steering optics (m) before traversing a 1-m-long field free-drift region (n). Ions are detected with a pair of microchannel plate detectors (o) and their arrival times are measured on a fast digital oscilloscope (LeCroy, Model 9350AM, 500 MHz). Resultant mass spectra are routinely collected over 2000 laser pulses.

All experiments are conducted using 10^{-2} M hydroquinone with once-distilled ethanol in deionized water (25% v/v EtOH in H_2O) as the solvent. Ethanol was used to prevent disintegration of the liquid filament upstream of the laser interaction region, an ongoing problem with pure water beams. Increasing the ethanol fraction between 25% v/v and 50% v/v provided no further improvement in LμJ stability, so the lower fraction was used throughout. Hydroquinone is used as supplied by the vendor without further purification (Aldrich, 99%).

3. Results and Discussion

3.1. The 1.9-μm Desorption/266-nm Ionization of Hydroquinone. A typical mass spectrum generated following the irradiation of a 10^{-2} M solution of hydroquinone (HQ) in 25% v/v ethanol in water is presented in Figure 2a. This mass spectrum was recorded with an IR desorption laser power of 1316 mJ cm^{-2} pulse^{-1} (0.19 GW cm^{-2}), and a time delay of 1 μs prior to UV ionization at a distance of 0.3 mm from the liquid beam. This time delay corresponds to the maximum in the two-laser-induced ion yield at the 0.3-mm separation and equates to a molecular desorption velocity of 300 ms^{-1}. The mass spectrum is entirely attributable to the ionization of neutral

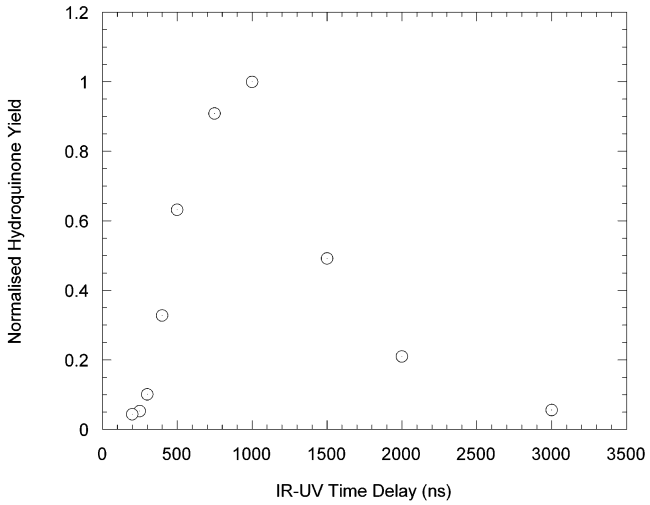

Figure 3. Hydroquinone parent ion yield recorded by ionizing desorbed molecules 0.3 mm from the liquid beam as a function of the IR−UV laser delay from 200 to 3000 ns (open circles). The longest laser delays ionize the slowest moving of the desorbed molecules. The diameter of the open circles represents the magnitude of the error in measuring ion yields.

hydroquinone molecules desorbed from the liquid beam. Under identical experimental conditions, except for the UV ionization laser being blocked, no ion signal is observed (Figure 2b), indicating that IR multiphoton absorption is not generating ions directly from within the liquid beam. Similarly, under conditions where the IR desorption laser is blocked but the ionization laser is maintained at a distance of 0.3 mm from the liquid beam, no ion signal is observed (Figure 2c). This latter observation indicates that the mass spectrum in the top trace of Figure 2 cannot be attributed to thermalized HQ molecules evaporating from the surface of the liquid beam and passing through the ionization volume of the UV laser.

The mass spectrum in Figure 2a clearly shows the HQ parent molecular ion at $m/z = 110$. Interestingly, no evidence for solvated HQ molecules is observed for m/z values greater than 110. The lack of solvated HQ clusters will be addressed later in this discussion, as will the significant width of the ion peaks. Extensive fragmentation of the parent ion is evident, with the most intense peak in the mass spectrum corresponding to $C_2H_3^+$ ions at $m/z = 27$. The presence of C^+ fragment ions at $m/z = 12$ indicates that complete fragmentation to atomic ions is occurring but is not a dominating photochemical pathway. Detailed discussions describing the photoionization and fragmentation processes in HQ have been previously reported and are not repeated here.[16,19]

3.2. Hydroquinone Desorption Velocity Distribution. We have investigated the time dependence of the HQ^+ parent ion yield by delaying the UV ionization laser pulse with respect to the IR desorption laser pulse by between 0.2 and 3 μs. The ionization laser was kept at a fixed distance of 0.3 mm away from the liquid beam, toward the ion detector, along the TOF axis (see Figure 1). Apertures in the ion extraction electrodes and entrance to the TOF mass spectrometer ensured that only those ionized species that were desorbed along an axis toward the ion detector enter the mass spectrometer. The desorption laser fluence was maintained at 2632 mJ cm^{-2} pulse^{-1}. The area of the parent HQ^+ ion signal was measured at each time delay and normalized to the largest peak area recorded. The normalized peak area values as a function of IR−UV laser delay time are presented as open circles in Figure 3. In Figure 4 the data has been inverted from IR−UV laser delay time to HQ

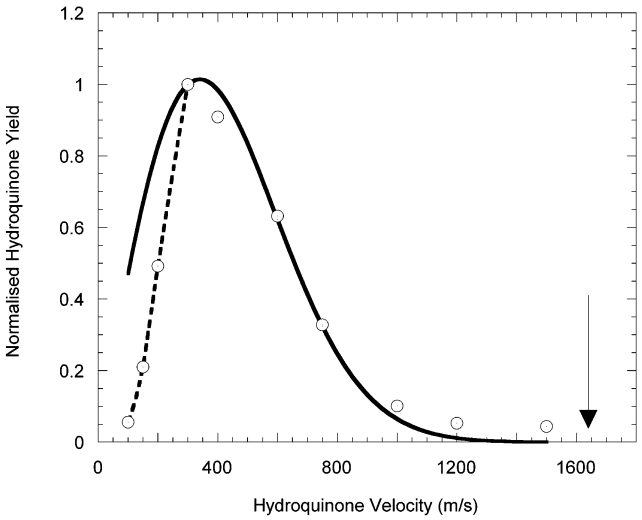

Figure 4. Hydroquinone parent ion velocity distribution determined by ionizing desorbed molecules 0.3 mm from the liquid beam as a function of the IR−UV laser delay from 200 to 3000 ns (open circles). The longest laser delays ionize the slowest moving of the desorbed molecules. The diameter of the open circles represents the magnitude of the error in measuring ion yields. The arrow to the right of the figure represents the speed of sound in 25% v/v EtOH in H_2O. The solid curve represents a nonlinear least-squares fit of a Boltzmann distribution to data points having a velocity of 300 m/s and greater. The temperature of this fit corresponds to hydroquinone having a translational temperature of 1538 ± 15 K. The dashed line highlights the mismatch between the observed and predicted (Boltzmann) ion yields for molecules desorbed at the lowest velocities. See text for a complete discussion.

(mass 110 amu) desorption velocity along the TOF axis. While the data presented in Figures 3 and 4 were collected with a desorption laser fluence of 2632 mJ cm^{-2} $pulse^{-1}$, an almost identical desorption velocity distribution was observed with a desorption laser fluence of 1316 mJ cm^{-2} $pulse^{-1}$.

Several comparisons of the data in Figure 4 can be made with the 1.9-μm desorption data for resorcinol previously reported by Kondow.[11,12] The first is that the peak in the HQ desorption velocity distribution observed in this study (300 ms^{-1}) is significantly slower than the average velocity of the fast-moving resorcinol molecules and clusters recorded by Kondow (1300 ± 100 ms^{-1}). Kondow notes that a desorption velocity of 1300 ms^{-1} corresponds to the speed of sound in aqueous resorcinol solution, suggesting that under the experimental conditions reported (we calculate Kondow's desorption fluence to be ∼130 mJ cm^{-2} $pulse^{-1}$), the fast-moving clusters are ejected via a compressive sound wave mechanism. The speed of sound in a solution of 25% v/v ethanol in water is approximately 1640 ms^{-1},[20] over 5 times higher than the maximum in the desorption velocity distribution recorded in this study, and is represented by the arrow in Figure 4. Clearly, even with the moderate velocity-resolving resolution available in this experiment (a 150-μm ionization cross section centered 300 μm from the liquid beam), the observed HQ desorption velocity distribution is well shifted to subacoustic velocities. An important conclusion of this work is that at the higher desorption fluxes used here, an acoustic shock wave mechanism is not operative. The desorption laser fluences employed in the cited studies, as well as those used here, are collated in Table 1. Together, these data suggest that the acoustic compression−ejection mechanism is operative only at low-desorption laser fluences.

Most recently, Kondow's group has reported that fast-moving neutral water clusters are generated following the relatively intense 2.96-μm irradiation of a liquid beam of water.[15] In this study, IR laser powers in the range 4.5−7 mJ $pulse^{-1}$ were used, but no focal spot size is reported, so the desorption fluences cannot be estimated. However, in support of the notion that the acoustic compression−ejection mechanism operates only at low-desorption laser fluences, these workers show that the abundance of slow-moving desorption species increases dramatically with laser power, while the abundance of fast-moving species remains a very minor desorption channel.

TABLE 1: Summary of IR Desorption Laser Fluences Used in This Study and in Closely Related Studies[a]

liquid-beam IR desorption study	desorption fluence (mJ cm^{-2} $pulse^{-1}$)	acoustic shock wave ejection
refs 11, 12: resorcinol @ 1.9 μm	∼130	yes
ref 13: phenol @ 2.92 μm	∼1100	no
this work: hydroquinone @ 1.9 μm	1316 and 2632	no

[a] The first column identifies the solute molecule and the IR desorption wavelength. The second column lists the estimated desorption laser fluence for each study. Finally, the third column identifies whether an acoustic shock wave ejection mechanism was observed.

Returning to the analysis of data in this study, we have estimated the translational temperature of the desorbed molecules. A normalized Maxwell−Boltzmann distribution that describes the desorption energy distribution at a temperature, T (Equation 1), is fitted to the data in Figure 4.

$$G(\epsilon)\mathrm{d}\epsilon = 2\pi\left(\frac{1}{\pi kT}\right)^{3/2}\sqrt{\epsilon}\,\exp\left(-\frac{\epsilon}{kT}\right)\mathrm{d}\epsilon \qquad (1)$$

The result of the best nonlinear least-squares fit to the Maxwell−Boltzmann distribution is represented by the solid line in Figure 4 and corresponds to a translational temperature of 1538 K for the HQ molecular mass of 110 amu. The most significant source of error in this determination, as discussed above, arises from the moderate velocity-resolving resolution in this experiment.

Figure 4 also contains a dashed line joining data points at the lowest cluster ejection velocities (longest IR−UV time delays). These low-velocity data points could not be fitted to a Maxwell−Boltzmann distribution without significantly degrading the quality of the fit to the overall data set. Qualitatively, we interpret this clearly non-Maxwell−Boltzmann behavior in terms of the lowest-energy desorbed species being barely able to overcome the attractive solvation forces at the surface of the liquid beam and therefore is released into the gas phase in lower yields than might otherwise be expected.

3.3. Indirect Evidence for the Desorption of Solvated Hydroquinone Clusters. We have previously reported on the photoionization and fragmentation behavior of HQ that has evaporated from the surface of a liquid beam[16] and note that the appearance of the mass spectrum in Figure 2a differs significantly from that previously reported. The differences in HQ mass spectra recorded under IR desorption and thermal evaporation conditions are presented in Figure 5. Figure 5a is simply a reproduction of the mass spectrum presented in Figure 2a. The mass spectrum in Figure 5b was recorded without the IR desorption laser pulse and increasing the gain on the microchannel plate ion detector to detect HQ molecules liberated via the lower-yield thermal evaporation process.

The most striking difference between the two mass spectra in Figure 5 is that almost all of the peaks in the IR desorption mass spectrum are significantly broader than those in the thermal evaporation mass spectrum. The sharp peaks in the lower trace result from the ionization of bare HQ solute molecules passing through the small UV laser focal volume. The extensive degree of fragmentation has previously lead us to conclude that at least four additional 266-nm photons following the ionization step

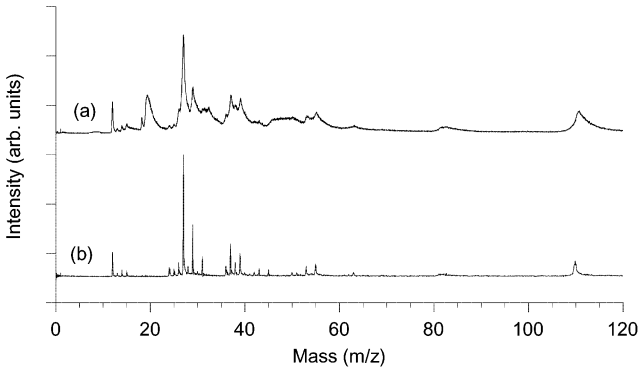

Figure 5. (a) IR (1.9-μm) desorption/UV (266-nm) ionization TOF mass spectrum of a 10^{-2} M solution of hydroquinone in 25% v/v ethanol in water. (b) Liquid beam/TOF mass spectrum of solute that has evaporated from a 10^{-3} M solution of hydroquinone in ethanol. See text for a complete discussion.

are being absorbed by the nascent HQ^+ ions.[16] Our current instrument is not equipped with a reflectron, and as such the linear TOF has a limited mass resolution. Nonetheless, the sharpness of the peaks ionized under thermal evaporation conditions highlights that the broad peaks observed following IR desorption are not attributable to the limited mass resolution of our apparatus.

Apart from most corresponding peaks in the IR desorption mass spectrum displaying a significantly greater width than those observed under thermal evaporation conditions, the former also display several additional broad peaks not observed under evaporation conditions. The most striking of these additional broad peaks is observed at $m/z = 19$ (where the baseline is flat under evaporation conditions), with additional, overlapping, and poorly resolved structure in the ranges $m/z \approx 25-34$, 36−44, 46−52 (again, where the baseline is almost entirely flat under evaporation conditions), and 53−58. We attribute the presence of these additional peaks as well as the unusual breadth of most peaks in the IR desorption mass spectrum to ionization, fragmentation, and high-energy photoinduced chemistry occurring within solvated HQ clusters desorbed from the liquid beam. The following paragraphs will address these inter-related processes in turn.

The first issue to be addressed is how can the appearance of the mass spectrum in Figure 5a be attributable to solvated HQ clusters when there is no mass spectral evidence for ions appearing at masses greater than the HQ^+ parent at $m/z = 110$? The IR desorption of solvated clusters from a liquid beam is not unprecedented. Kondow has reported that fast-moving resorcinol clusters desorbed from the surface of a liquid beam of water are stabilized by solvent evaporation prior to ionization.[11,12] It is reasonable to assume, therefore, that in this study solvated HQ clusters desorbed from the liquid beam also give up internal energy to evaporation as they move toward the ionization volume, and we might reasonably expect to observe solvated clusters in the mass spectrum. However, the absence of such species can be explained by considering the energetics of the HQ photoionization process.

The HQ molecules are ionized via 1+1 REMPI using 266-nm (4.6 eV) photons. As such, the total two-photon excitation energy is 9.2 eV. The ionization potential (IP) of HQ has been determined by several different methods and is reported to be 7.93, 7.94, 7.95, or 8.44 eV.[21] If we ignore the large outlier value and take the next highest IP of 7.95 eV, each HQ^+ ion has as much as 10 080 cm^{-1} of excess internal energy to be accounted for following ionization. This maximum amount of excess energy corresponds to the concomitant generation of photoelectrons with zero kinetic energy. Typical binding energies for small aromatic-water clusters are about 500−2000 cm^{-1},[22] indicating that HQ^+* (here the asterisk is used to identify energetically excited ions) has sufficient excess internal energy to overcome several, perhaps up to five, solute−solvent bonds. Fewer solute−solvent interactions could be overcome if the nascent photoelectrons carry away a considerable fraction of the 10 080 cm^{-1} as kinetic energy. Therefore, a more likely explanation for complete cluster dissociation is the additional photoabsorption that occurs following ionization. This additional absorption has already been attributed to the extensive HQ fragmentation evident in Figure 5b. Fragment ions observed at $m/z \approx 12-15$, 25−34, 36−44, 53−58, and 81 in Figure 5a can therefore be attributed to the high-energy fragmentation pathways previously reported.[16]

Having solvated clusters of HQ molecules desorbed from the liquid beam is an appealing interpretation of the dynamics of the IR desorption process in that it now allows for a ready explanation of the unusually broad parent and fragment ion peaks in Figure 5a. Our experiment ionizes only those desorbed species that travel from the liquid beam along the TOF axis toward the mass spectrometer. Once ionized, any solvated HQ^+* clusters that release their excess internal energy via solvent dissociation along the TOF axis will liberate bare HQ^+ ions possessing additional kinetic energy components directed both toward and away from the ion detector. As such, HQ^+ ion arrival times will be smeared out from those observed following ionization of the bare solute molecules evaporated from the liquid surface. Excess-energy-induced dissociation of the solvent from clusters containing HQ fragment ions also accounts for the unusual breadth of the lower mass peaks.

With respect to Figure 5, what remains to be explained is the appearance of peaks in the IR desorption mass spectrum that do not appear in the thermal evaporation mass spectrum, namely, peaks at $m/z = 18$, 19−20, and 46−52. We attribute the additional peaks in the IR desorption spectrum to UV-laser-induced intracluster reaction products. The small, sharp peak at $m/z = 18$ is H_2O^+, created by an evaporative charge transfer to solvent process involving HQ^+* (or a fragment thereof) that has absorbed at least one additional photon following the initial ionization event (water has an ionization potential of 12.62 eV[21]). The more intense broad peak at $m/z = 19-20$ is attributed to $H^+ \cdot H_2O$. Finally, the broad collection of peaks at $m/z = 46-52$ most likely arises from ionization of ethanol solvent from within the desorbed HQ clusters (ethanol is present in the liquid beam at 25% v/v), as well as protonated ethanol clusters, $H^+ \cdot$ EtOH. The lack of mass resolution in this region of the mass spectrum makes it difficult to comment further on the identity of these peaks. Nonetheless, Kondow has previously reported the generation of similar charged species following the direct UV irradiation of an ethanol liquid beam.[23]

We have already estimated from our IR−UV time delay studies that HQ molecules desorbed from the liquid beam possess a translational temperature of ~1500 K. For larger solvated cluster masses, correspondingly higher translational temperatures result. This indicates that desorbed clusters must be ejected under thermodynamic nonequilibrium conditions as fast moving, internally cold species. Internal energies corresponding to temperatures >1500 K would be sufficiently high to overcome the noncovalent cluster binding energies. Indeed, IR desorption of nonvolatile molecules from a liquid beam can probably be described as being analogous to the matrix-assisted laser desorption/ionization (MALDI) process where a "cold"

matrix is employed. A cold MALDI matrix promotes the ejection of large solute molecules, particularly biomolecules, into the gas phase with a relatively low deposition of internal energy.[24,25] Such an analogy is also consistent with data from Faubel[26,27] and Brutschy's[14] laboratories where aqueous liquid beams are estimated to be cooled by as much as ~60 K from ambient. Nonetheless, further study is required to better understand the mechanism of IR desorption from liquid beams.

4. Conclusions

We have investigated the 1.9-μm IR desorption of HQ in a water/ethanol liquid beam under relatively high desorption laser fluences (1316 and 2632 mJ cm^{-2} $pulse^{-1}$). The maximum in the hydroquinone desorption velocity distribution is 300 ms^{-1}, and the translational temperature of the desorbed species is approximately 1500 K. We see no evidence for an acoustic compression−ejection mechanism usually observed under more mild desorption conditions and suggest that this mechanism is only operative at relatively low-desorption laser fluences. The appearance of the IR desorption/UV ionization TOF mass spectrum of HQ is interpreted in terms of dissociation of solvated HQ clusters during the ionization event. Our results suggest a general mechanism for the high-powered IR desorption from a liquid beam whereby desorbed species are ejected into the vacuum possessing considerable translational energy but remain internally cool.

Acknowledgment. The University of Adelaide, the Australian Research Council (ARC), the South Australian Department of Mines and Energy through the State Energy Research Advisory Committee (SENRAC), and the Australian Land and Water Resources Research and Development Corporation (LWRRDC) have supported this work. The technical support provided by the University of Adelaide Mechanical, Electronics, and Glassblowing Workshops is gratefully acknowledged. Helpful discussions with Prof. W. D. Lawrance are gratefully acknowledged. D.E.O. thanks the University of Adelaide for an International Student Honors Award.

References and Notes

(1) Kondow, T.; Mafuné, F. *Annu. Rev. Phys. Chem.* **2000**, *51*, 731−761 (and references therein).

(2) Kleinekofort, W.; Pfenninger, A.; Plomer, T.; Griesinger, C.; Brutschy, B. *Int. J. Mass Spectrom. Ion Processes* **1996**, *156*, 195−202.

(3) Kleinekofort, W.; Avdiev, J.; Brutschy, B. *Int. J. Mass Spectrom. Ion Processes* **1996**, *152*, 135−142.

(4) Kleinekofort, W.; Schweitzer, M.; Engels, J. W.; Brutschy, B. *Int. J. Mass Spectrom. Ion Processes* **1997**, *163*, 1L−4L.

(5) Sobott, F.; Kleinekofort, W.; Brutschy, B. *Anal. Chem.* **1997**, *69*, 3587−3594.

(6) Sobott, F.; Schunk, S. A.; Schüth, F.; Brutschy, B. *Chem. Eur. J.* **1998**, *4*, 2353−2359.

(7) Sobott, F.; Wattenberg, A.; Kleinekofort, W.; Pfenninger, A.; Brutschy, B. *Fresenius' J. Anal. Chem.* **1998**, *360*, 745−749.

(8) Wattenberg, A.; Barth, H.-D.; Brutschy, B. *J. Mass Spectrom.* **1997**, *32*, 1350−1355.

(9) Wattenberg, A.; Sobott, F.; Barth, H.-D.; Brutschy, B. *Eur. Mass Spectrom.* **1999**, *5*, 71−76.

(10) Wattenberg, A.; Sobott, F.; Brutschy, B. *Rapid Commun. Mass Spectrom.* **2000**, *14*, 859−861.

(11) Horimoto, N.; Kohno, J.; Mafuné, F.; Kondow, T. *J. Phys. Chem. A* **1999**, *103*, 9569−9572.

(12) Horimoto, N.; Kohno, J.; Mafuné, F.; Kondow, T. *Chem. Phys. Lett.* **2000**, *318*, 536−542.

(13) Kohno, J.; Mafuné, F.; Kondow, T. *J. Phys. Chem. A* **2001**, *105*, 8939−8943.

(14) Wattenberg, A.; Sorbott, F.; Barth, H.-D.; Brutschy, B. *Int. J. Mass Spectrom.* **2000**, *203*, 49.

(15) Kohno, J.; Mafuné, F.; Kondow, T. *Chem. Lett.* **2002**, 562−564.

(16) Holstein, W. L.; Hammer, M. R.; Metha, G. F.; Buntine, M. A. *Int. J. Mass Spectrom.* **2001**, *207*, 1−12.

(17) Holstein, W. L.; Hayes, L. J.; Robinson, E. M. C.; Laurence, G. S.; Buntine, M. A. *J. Phys. Chem. B* **1999**, *103*, 3035−3042.

(18) Siegman, A. E. *Lasers*; University Science Books: Mill Valley, CA, 1986.

(19) Akopyan, M. E.; Kleimenov, V. I.; Feofilov, A. G. *High Energy Chem.* **2000**, *34*, 107−111.

(20) Martin, K.; Spinks, D. *Ultrasound Med. Biol.* **2001**, *27*, 289−291.

(21) Linstron, P. J., Mallard, W. G., Eds. *NIST Chemistry WebBook*; NIST Standard Reference Database Number 69; National Institute of Standards and Technology: Gaithersburg, MD, March 2003 (http://webbook.nist.gov).

(22) Zwier, T. S. *Annu. Rev. Phys. Chem.* **1996**, *47*, 205−241.

(23) Mafuné, F.; Kohno, J.; Kondow, T. *J. Phys. Chem.* **1996**, *100*, 10041−10045.

(24) Beavis, R. C.; Lindner, J.; Grotemeyer, J.; Schlag, E. W. *Chem. Phys. Lett.* **1988**, *146*, 310−314.

(25) Medzihradszky, K. F.; Campbell, J. M.; Baldwin, M. A.; Falick, A. M.; Juhasz, P.; Vestal, M. L.; Burlingame, A. L. *Anal. Chem.* **2000**, *72*, 552−558.

(26) Faubel, M.; Schlemmer, S.; Toennies, J. P. *Z. Phys. D* **1988**, *10*, 269−277.

(27) Faubel, M.; Steiner, B.; Toennies, J. P. *J. Chem. Phys.* **1997**, *106*, 9013−9031.